

## Highly active photocatalytic paint for NO<sub>x</sub> abatement under real-outdoor conditions

Joana Ângelo, Luísa Andrade, Adélio Mendes\*

LEPABE - Faculdade de Engenharia, Universidade do Porto, rua Dr. Roberto Frias, 4200-465 Porto, Portugal

### Abstract

In this work the photocatalytic activity of paints incorporating commercial titanium dioxide for outdoor nitrogen oxide (NO) photoabatement is assessed. The paint acts as a 3D support of the photocatalyst and thus allows a larger amount of TiO<sub>2</sub> nanoparticles to absorb light and to contact with pollutants, when compared with a 2D photocatalytic surface. NO conversion and selectivity towards nitrites and nitrates were determined according to the standard ISO 22197-1:2007 (E). Paint coatings were formulated and tested under laboratory and outdoor conditions. The best paint formulation incorporates CristalACTiV™ PC500 photocatalyst from Cristal and calcium carbonate extender, presenting a NO conversion of ca. 70% and a selectivity of ca. 40% under laboratory conditions. The same photocatalyst but characterized in the form of an optically thick film of compressed powder presented ca. 95% and 45% of conversion and selectivity, respectively. Under the real-outdoor conditions, the best performing paint showed a NO conversion of about 95%.

### 1. Introduction

NO<sub>x</sub> pollution is responsible for well-known environmental problems such as production of tropospheric ozone, acid rains and global warming but it can also affect humans health, in particular the respiratory and immune systems. Thus, specific regulations to control this kind of emissions were established by EPA [1] in USA and by EEA [2] in Europe. Both EPA and EEA established the hourly NO<sub>x</sub> air concentration limit at 0.1 ppm and 0.2 ppm, respectively. Even though processes such as selective catalytic and non-catalytic reduction of NO<sub>x</sub> were implemented to reduce the end of pipe emissions [3,4], photocatalysis with titanium dioxide (TiO<sub>2</sub>) is now being seen as a very promising approach to decompose these pollutants [5–7]. In fact, solar photoabatement of pollutants uses the sun as energy source and works at atmospheric conditions degrading pollutants present in low atmospheric concentrations. Photocatalysis is able to oxidize a wide spectrum of contaminants, not requiring any additional chemicals and using a relative low-cost material [6,8,9]. During a photocatalytic process, the semiconductor exposed to sunlight radiation absorbs photons with energy higher than its band gap and injects electrons from the valence to the conduction band, creating electron-hole pairs. The holes have a onto the semiconductor surface to OH• radicals. On the other hand, excited electrons react with oxygen molecules to form the superoxide anions O<sub>2</sub>•–; then radicals OH• oxidize contaminants, namely nitrogen oxides.

Several materials incorporating photocatalytic titanium dioxide used for air purification were already reported, e.g. tiles, cement mortars and paints [10]. Mortars and paint coatings are the building materials most used for this kind of applications [11–16]. Although several works study the photoabatement of NO<sub>x</sub> under lab conditions, there is a lack of studies reporting NO<sub>x</sub> photoabatement under real outdoor conditions. For instance, part of Borgo Palazzo Street in Bergamo, Italy, was covered with photocatalytic paving stones (stones coated with TX Active® produced by *Italcementi*) and NO<sub>x</sub> concentration was measured during two weeks. The results

were critically compared with the unmodified fraction of the street, paved with asphalt. The surrounding air of the photocatalytic pavement showed a NO<sub>x</sub> concentration of ca. 30–40% smaller than the reference values [17]. A similar project was developed in Antwerp. An area of 10 000 m<sup>2</sup> was coated with photocatalytic pavement blocks and the correspondent efficiency towards NO<sub>x</sub> photoabatement was assessed. Although the results showed a decrease in NO<sub>x</sub> concentration, it was not possible to withdraw sound conclusions since the measurements were made only during a very small period of time. Laboratory tests were then performed to prove the photocatalytic efficiency of this pavement blocks over time and the results were very promising [18]. The efficacy of NO<sub>x</sub> photoabatement using TiO<sub>2</sub>-mortar panels (also coated with TX Active®) was tested in outdoor conditions in France [19]. In this case study, three artificial canyon streets were constructed and NO<sub>x</sub> concentration levels monitored. The canyon streets covered with TiO<sub>2</sub>-mortar panels showed NO<sub>x</sub> photoabatement values in the range of 37–82%, depending on the pollutant concentration, wind direction and sun- light orientation [19]. Other very interesting projects developed under outdoor conditions were performed to foster the use of photocatalytic paints as a possible solution to overcome imminent environmental problems. For instance, Umberto I Tunnel in Rome, Italy, was coated with a photocatalytic paint (cement-based paint with TX Active®) and outfitted with an artificial UV lighting system. This study reported values of more than 20% of NO<sub>x</sub> reduction [20]. Boysen® KNOxOUTTM is a well-known photocatalytic commercial paint that can be used both for indoor (acrylic-based paint) and outdoor (silicone-based paint) applications. An indoor paint loaded with this photocatalyst was used to coat the Vinci Car Park in Paris, France. An area of about 1800 m<sup>2</sup> was coated and illuminated using fluorescent lights; a decrease of 90% of the NO<sub>x</sub> concentration was observed [21]. On other hand, Maggos et al. [22] reported 20% NO<sub>x</sub> reduction in a car parking coated with a photocatalytic paint and illuminated with UV lamps. In what concerns outdoor applications, Allen et al. [23] reported a pilot study of NO<sub>x</sub> photoabatement in the playground of Sir John Cass School, in London, UK. The playground with an area of 300 m<sup>2</sup> was painted with photocatalytic paint Boysen® KNOxOUTTM and the NO<sub>x</sub> concentration measured during 6 months; though assessing the photocatalytic paint role is very difficult due to the very open nature of the playground, it was possible to observe a decrease in the NO<sub>x</sub> levels [23,24]. Ongoing project EDSA – “Everyone Deserves Safe Air”, by Boysen Paints company in Philippines, coordinated by the Metro Manila Development Authority and curated by TAO Incorporation, aims at reducing outdoor atmospheric pollution using artistic features [21,25]. Project Light2Cat concerned the development of a modified TiO<sub>2</sub> photocatalyst active under visible and UV light. The new photocatalyst, which can be incorporated in building elements such as concrete, was optimized to respond under typical solar radiation of a large range of latitudes [26]. More recently, Suárez et al. [27] described a new experimental setup for testing photocatalytic materials, SYPHOMA. This experimental setup allows determining the photocatalytic activity under sunlight for treating outdoor polluted air; it was assessed for NO<sub>x</sub> photoabatement using photocatalytic-coated asphalts. NO<sub>x</sub> concentrations, relative humidity, irradiance and temperature are recorded during all the experiments. All these efforts on assessing results under real-field applications foster the use of photocatalytic materials as an important agent to reduce pollutants concentrations in the air.

Considering the specific application of NO degradation, photocatalytic paints show two main advantages when compared with other kind of construction supports. Paint coatings can be applied in different constructive elements, such as streets, buildings, tunnels, and they present the advantage of being a 3D layer where TiO<sub>2</sub> nanoparticles are available for photocatalysis up to the paint film optic thickness, ca. 100 µm. A photocatalytic paint coating has a very large interfacial area available for photocatalysis, originating then very photoactive surfaces to degrade pollutants. Even though titanium dioxide is one of the major components on the formulation of a paint (its function is to give opacity to the paint), this titanium dioxide is pigmentary, mainly in rutile phase for preventing any photoactivity. Consequently, the paint formulation needs to be modified for incorporating photocatalytic titanium dioxide, normally or essentially, anatase. The presence of pigmentary TiO<sub>2</sub> in paints jeopardizes the photoactivity because it acts as a blocking agent for the solar radiation resulting in low levels of NO conversion and selectivity [28]. Thus, pigmentary TiO<sub>2</sub> should be removed from the paint formulation and replaced by extenders, which are beneficial for the photoactivity of the paint film. In the present work, an exterior water-based paint was formulated to incorporate two commercial photocatalysts: P25 from Evonik and PC500 from

Cristal. The photocatalysts were characterized in powder form [28] and after incorporation in the formulated paint; the photocatalytic activity was assessed according to standard ISO 22197-1:2007 [“Fine ceramics (advanced ceramics, advanced technical ceramics) – Test method for air-purification performance of semiconducting photocatalytic materials – Part 1: Removal of nitric oxide”] and under real-outdoor conditions.

## 2. Experimental

### 2.1. Photocatalytic films

Two samples of commercial photocatalytic titanium dioxide were tested for NO photoabatement: P25 from Evonik and PC500 from Cristal. The photocatalysts properties are detailed in Table 1. The above described photocatalysts were then incorporated in a paint coating and characterized to assess photo-oxidation of NO. The developed photocatalytic paint was optimized from a commercial exterior water-based paint (vinyl paint) described elsewhere [29]. The main components of this commercial paint are: pigmentary TiO<sub>2</sub> (18 wt.%), water (30 wt.%), extenders (18 wt.%: CaCO<sub>3</sub> and silicates), polymer extender slurry (8 wt.%), binder slurry (20 wt.%) and additives slurry (6 wt.%). This paint has high porosity due to a pigment volume concentration (PVC) slightly above the critical value (CPVC), thus allowing the easy access of the photocatalyst to the pollutant. Four different paint formulations were tested– Table 2 – loaded with two different commercial photocatalysts, P25 and PC500. The commercial vinyl paint has 18 wt.% of pigmentary TiO<sub>2</sub> in wet basis; this paint is hereafter named as Reference Paint (RP). The maximum photocatalyst content incorporated in the formulated paints was 9 wt.% (wet base): paints #1 and #3 contained 9 wt.% of pigmentary TiO<sub>2</sub> and 9 wt.% of photo- catalytic TiO<sub>2</sub>, while paints #2 and #4 contained 9 wt.% of calcium carbonate instead of the pigmentary TiO<sub>2</sub>. The paint films were applied on aluminum slabs of 10 cm 5 cm with a wet thickness of 200 μm.

**Table 1**  
Photocatalyst properties provide by manufacturers.

	P25	PC500
Manufacturer	Evonik	Cristal
Crystal structure	~80% anatase/~20% rutile	>99% anatase
Crystal size (nm)	25	5–10
Shape	Primary particles	Agglomerates
Surface area	50	345
Agglomerate size (μm)	n.p.	1.2–1.7

**Table 2**  
Paint reformulation composition.

Paint	Components			
	Pigmentary TiO <sub>2</sub>	CaCO <sub>3</sub>	P25	PC500
Reference paint	18 wt.%			
#1	9 wt.%		9 wt.%	
#2		9 wt.%	9 wt.%	
#3	9 wt.%			9 wt.%
#4		9 wt.%		9 wt.%

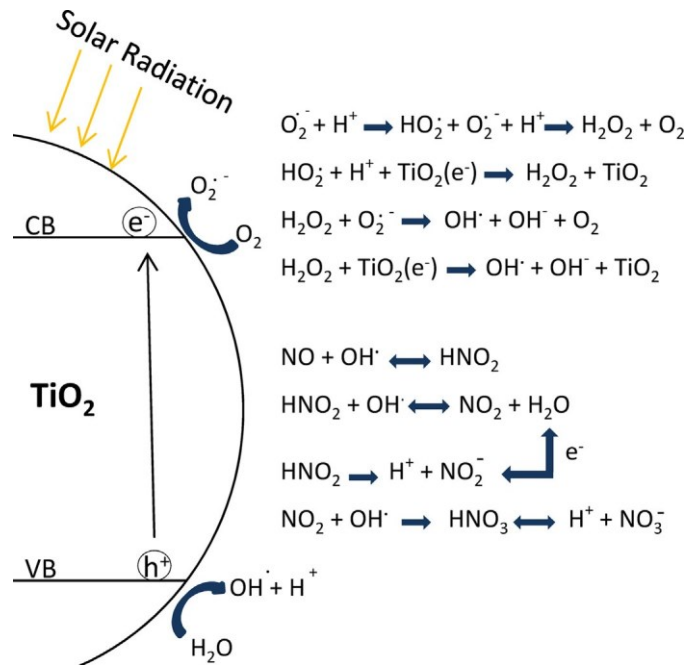


**Fig. 1.** Mechanism of photocatalysis with main reactions.

## 2.2. Photocatalytic tests

The performance of the photocatalyst was characterized by two parameters: conversion of NO (Eq. (1)) and selectivity to the formation of ionic species (Eq. (2)):

$$X_{NO} = \left( \frac{c_{NO}^{in} - c_{NO}^{out}}{c_{NO}^{in}} \right) \quad (1)$$

$$S = \left( 1 - \frac{c_{NO_2}^{out}}{c_{NO}^{in} - c_{NO}^{out}} \right) \times 100 \quad (2)$$

where  $X_{NO}$  is the conversion of NO,  $S$  is the selectivity to the formation of ionic species,  $C_{NO}$  and  $C_{NO_2}$  stand for the concentration of NO and  $NO_2$ , respectively, and the superscripts (in and out) refer to the reactor's inlet and outlet streams. The radicals  $OH\cdot$  are responsible for the oxidation of contaminants, as mentioned previously. When NO reacts with  $OH\cdot$  some species can be formed, such as  $HNO_2$  ( $H+NO_2^-$ ),  $HNO_3$  ( $H+NO_3^-$ ) and  $NO_2^-$  - Fig. 1. Since  $NO_2$  is even more harmful than NO to human health, the desired reaction products are the ionic species ( $NO_2^-$  and  $NO_3^-$ ).

### 2.2.1. Experimental setup

An experimental setup based on standard ISO 22197-1:2007 ["Fine ceramics (advanced ceramics, advanced technical ceramics) - Test method for air-purification performance of semiconducting photocatalytic materials - Part 1: Removal of nitric oxide"] was used to evaluate the photocatalytic activity of powder pressed and paint films. This setup consists of four main sections: (i) feed, (ii) reactor, (iii)  $NO_x$  quantification and (iv) computer monitoring/control - Supplementary information Fig. S1.

In the first section, the gas stream with the desired NO concentration, relative humidity and flow

rate, is prepared and fed to the photoreactor. The feeding system consists of a flow controller of NO (MFC 0–0.1 L<sub>N</sub> min<sup>-1</sup> – Hi-Tech Bronkhorts), two flow meters for dry and wet air (MFM 0–1 L<sub>N</sub> min<sup>-1</sup> – Hi-Tech Bronkhorts), respectively, and a bubbler used to humidify the dry air (100% relative humidity under test temperature and feed flow rate); the latter allows to obtain a stream at any relative humidity between 0 and 100%.

The reaction section is composed by a photoreactor (with a Pyrex® window) designed to hold the samples, minimizing dead and stagnant volumes. Above the reactor is the UV lamp (Vilbert Lourmat – BLB 365 nm, 2 lamps of 6 W each), which distance to the photoreactor window can be varied. NO and NO<sub>2</sub> concentrations are quantified using a chemiluminescence analyzer (Thermo Electron 42C), as suggested in the standard. A computer controls the experimental set-up and acquires the relevant data. The reactor is placed inside a thermostatic cabin to ensure controlled and constant temperature. Photocatalytic tests were performed at a feed rate of 0.7 L min<sup>-1</sup> of NO at 1 ppmv in air and 50% of relative humidity, at 25 °C with an irradiance of 10 W m<sup>-2</sup>.

### 2.2.2. Outdoor experimental setup

An outdoor experimental setup was designed and assembled to determine the NO<sub>x</sub> photoabatement efficiency of photocatalytic paints when irradiated directly by sunlight – Supplementary information Fig. S2.

This setup comprises also four main sections: (i) feed, (ii) reactor, (iii) NO<sub>x</sub> quantification and (iv) computer acquisition and control. A NO stream in air (ca. 150–200 ppbv) was fed to the reactor. The photoreactor is made of acrylic material with a Pyrex® window. The paint samples are applied in a fiber cement board (70 cm 20 cm, Supplementary information Fig. S3) and they are placed on the back of the photoreactor. The flow passes through the reactor contacting with the samples; NO concentration is then quantified using a chemiluminescence analyzer (Thermo Electron 42C) and all the experiments are controlled using a computer.

### 2.3. Diffuse reflectance analyses

Diffuse reflectance spectroscopy can be used to obtain the absorption properties of crystalline and amorphous materials [30,31]. The band gap of a sample can be obtained from the Tauc equation, which relates the diffuse reflectance and the Kubelka–Munk model with the excitation frequency [31]:

$$(hvF(R_{\infty}))^{\frac{1}{n}} = A(hv - E_g) \quad (3)$$

where  $h$  is Planck's constant,  $\nu$  is frequency of vibration,  $A$  is a proportional constant and  $E_g$  is the band gap. This equation is obtained by multiplying the Kubelka–Munk equation by the energy of the incident radiation ( $E = h\nu$ ) and powered to a coefficient  $n$ , according to the type of the electronic transition of the material. For indirect transitions,  $n$  equals 2 and for direct transition  $n$  is 1/2. Plotting the modified Kubelka–Munk equation as a function of the incident radiation ( $E$ (eV)), the band gap of the semiconductor can be obtained extrapolating the linear part of this curve to the x-axis, the so-called Tauc plot; the band gap energy is read at the intersection. Diffuse reflectance of the different samples were obtained in a Shimadzu UV-3600 UV-VIS-NIR spectrophotometer, equipped with a 150 mm integrating sphere and using BaSO<sub>4</sub> as 100% reflectance standard. The samples were pressed to form a flat disc that fit into the spectrophotometer sample holder.

### 2.4. SEM and XRD analyses

The morphology and composition of the photocatalysts and photocatalytic paints were obtained from scanning electron microscopy (SEM) coupled with energy dispersive X-ray (EDX) analysis. A FEI Quanta 400FEG ESEM/EDAX Genesis X4M apparatus equipped with a Schottky field emission gun (for optimal spatial resolution) was used for the characterization of the surface morphology of the photocatalysts powders and for photocatalytic paints. These SEM/EDX

analyses were made at CEMUP (Centro de Materiais da Universidade do Porto). The crystallographic characterization of samples was obtained using the X-ray diffraction (XRD). The XRD pattern of the selected samples was collected using a Denchtop X-Ray Diffractometer RIGAKU, model MiniFlex II using Cu X-ray tube (30 KV/15 mA). The data was collected at 20 angles (10–80°), with a step speed of 3.5°/min. Debye–Scherrer equation was used to determine the crystallite size. The obtained X-ray scans were compared to those of standard database and the phases were assigned comparing with data available in literature.

## 2.5. UVCON – accelerated aging tests

Accelerated aging tests are a fast approach to evaluate the durability of paints when exposed to sunlight and humidity. These accelerated aging tests were performed according to standard ISO 11507:2011 with UVA-340 lamps (QUV-A test). A typical accelerated aging test performed in the paint industry is UVCON. This test aims to evaluate the paint film degradation caused by exposure to sunlight and water condensation. It is important to mention that there is no direct correlation between the UVCON results and the real behavior of paints under outdoor conditions, though it gives useful information about the kind of damages that often can occur. These damages are mainly color change, gloss loss, chalking and cracking.

## 3. Results and discussion

### 3.1. Photocatalytic paint films

The photocatalytic activity for NO abatement was obtained for the four prepared paints, applied in aluminum slabs of 10 cm × 5 cm. The correspondent results are shown in Fig. 2.

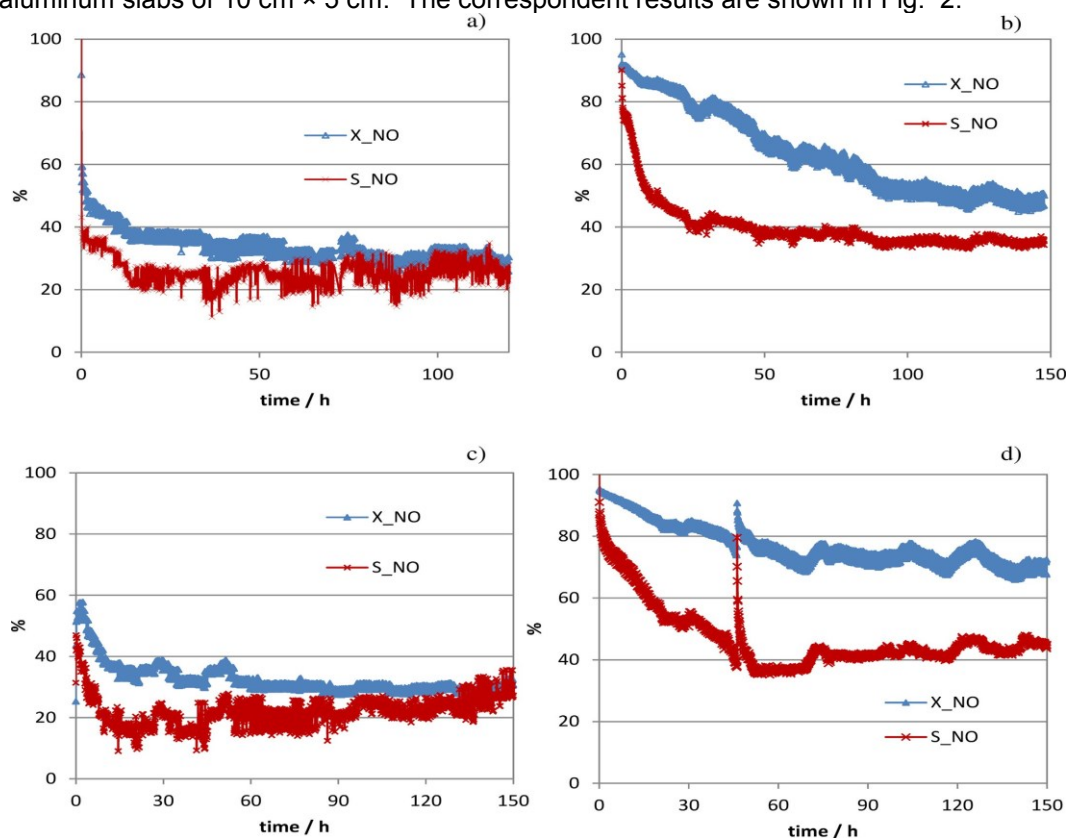


**Fig. 2.** NO conversion (XNO) and selectivity (S) histories for paints #1 (a), #2 (b), paints #3 (c) and #4 (d). Photocatalytic tests were performed at a feed rate of 0.7 L min<sup>-1</sup> of NO at 1 ppmv in air and 50% of relative humidity, at 25 °C with an irradiance of 10 W m<sup>-2</sup>.

Calcium carbonate was selected as extender to be integrated in these formulations because it is a cheap material usually used in commercial paint formulations; it is more transparent to the UV light than the pigmentary  $\text{TiO}_2$  and reacts with nitrate compounds, producing calcium nitrates that are easily washed off from the paint surface. Indeed, the NO conversion is favored since calcium carbonate assists the removal of nitrates from the photocatalyst surface, which are products of the NO photooxidation.

Analyzing Fig. 2, it is possible to conclude that Paint #3 with 50% of pigmentary  $\text{TiO}_2$  and 50% of PC500 shows better performance at steady-state conditions (conversion of 30% and selectivity of 30%) than Paint #1, which incorporates P25 instead of PC500 (conversion of 25% and selectivity of 25%). These results are in agreement with the ones obtained for compressed powder films reported in a previous work [28]. Moreover, a higher photocatalytic activity of paints incorporating PC500 was already expected because the surface area of PC500 photocatalyst is six times higher than P25. Paints #2 and #4, formulated without pigmentary  $\text{TiO}_2$ , showed a significantly higher photoactivity; in particular Paint #4, loaded with PC500, showed the highest performance (conversion of 70% and selectivity of 45%), followed by Paint #2 loaded with P25 (conversion of 50% and selectivity of 35%). In fact, Paint #4 presented a very interesting photocatalytic activity, comparable to the photo activity of the corresponding compressed power film, reported elsewhere [28].

For comparison purposes, two commercial photocatalytic paints, Fotodecor and Fotosilox (from company Global Engineering acquired on 2010), were also tested under the same conditions and no significant conversion was observed Fig. 3.

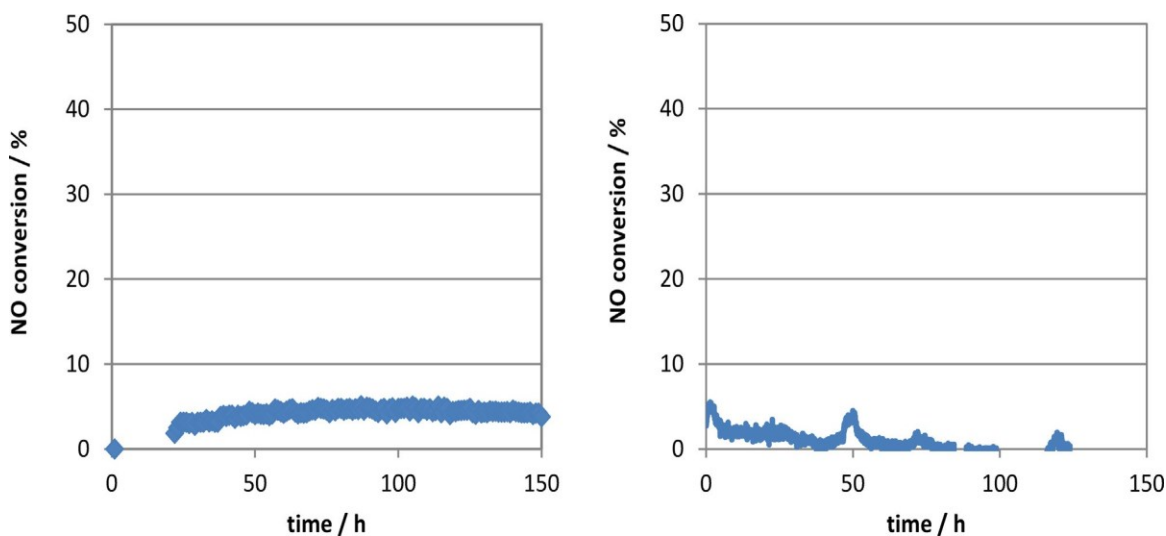


**Fig. 3.** NO conversion for Fotodecor and Fotosilox (Global Engineering), commercial paints. Photocatalytic tests were performed at a feed rate of  $0.7 \text{ L min}^{-1}$  of NO at 1 ppmv in air and 50% of relative humidity, at  $25^\circ\text{C}$  with an irradiance of  $10 \text{ W m}^{-2}$ .

The reference paint (RP) and the four formulated paints were tested in the outdoor experimental setup – Supplementary information Fig. S2 – and the correspondent NO conversion was evaluated. Outdoor experiments lasted about 5 h. First, NO feeding concentration (with a NO feed of about 100 ppbv and with no paint sample) was obtained for 2 h. Then, the paint sample was placed in the setup and tested during 3 hours; at the end, the paint sample was removed and the NO concentration obtained for more ca. 60 min. This allowed to check the stability of the NO analyzer. The outdoor photoreactor was placed in Porto city ( $41^\circ 11' \pm \text{N}$ ,  $8^\circ 36' \pm \text{W}$ ) and run on February and March of 2013. The NO content in the ambient air was observed to vary significantly with the time, making it difficult to compare the performances of the tested samples. A stable NO feed stream was then fed to the photoreactor (NO concentration was 100 20 ppbv). As expected, the reference paint exhibited no photoactivity (Fig. 4).

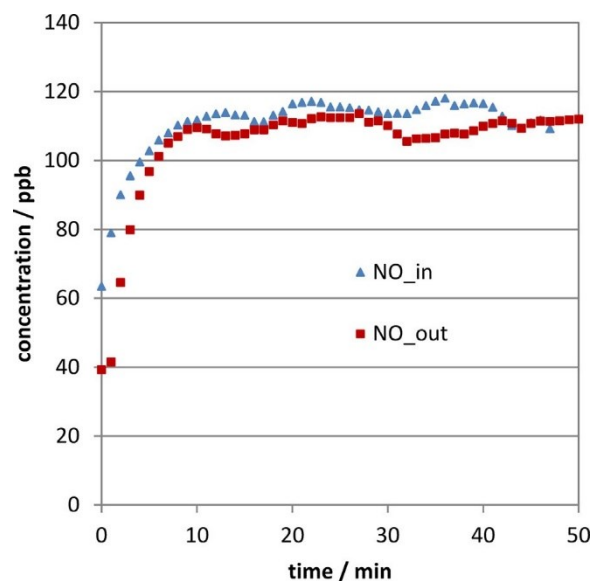


**Fig. 4.** Feeding in NO concentration (NO in) and venting out NO concentration (NO out) history for the reference paint (RP).

The histories of NO concentration during the three stages of the photocatalytic experiments are shown in Fig. 5: (i) the feeding concentration (NO in); (ii) venting concentration when the paint sample was in place (NO out during 200 min); and (iii) venting out concentration after removing the paint sample (NO out during ca. 60 min). The vertical red line in Fig. 5 marks the moment when the sample is removed. The results for NO conversion for the four paints are plotted in Fig. 6.

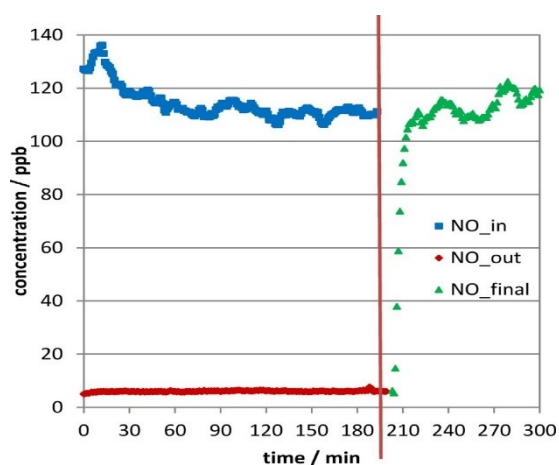


**Fig. 5.** NO concentration histories for the reference paint sample: NO<sub>in</sub> feed in concentration; NO<sub>out</sub> venting out concentration with paint sample; NO<sub>final</sub> venting out concentration without paint sample. The vertical line marks the end on the experiment with the paint sample. (For interpretation of the references to color in this figure legend, the reader is referred to the web version of the article.)

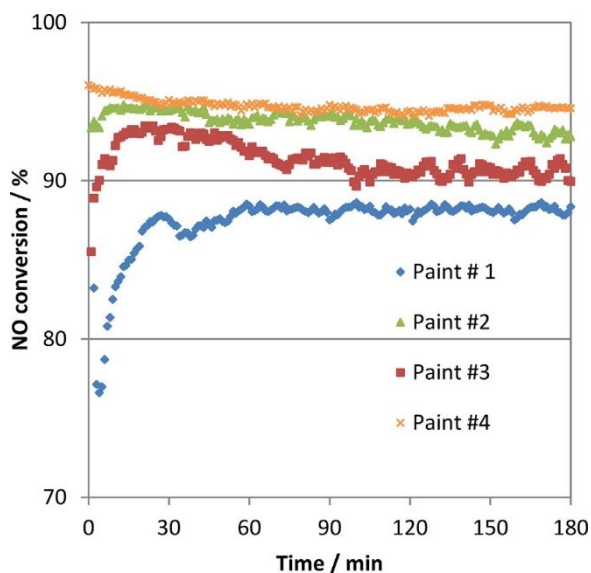


**Fig. 6.** NO conversion ( $X_{NO}$ ) for the four tested paints.

All the tested paints showed very good NO conversions, higher than 80%. As for the lab results, the performance of the paint samples are from the best to the worst as follows: paints #4, #2, #3 and #1, even though the differences are not as notorious as for the lab results. Paint #4 showed a very high and stable NO conversion (ca. 95% of conversion). The outdoor test unit has an average residence time of ca. 14 min, significantly higher than the residence time for the lab unit, 2.1 s, justifying the differences in conversion observed.

### 3.2. Diffuse reflectance analyses

The diffuse reflectance was obtained for photocatalysts P25 and PC500, Fig. 7, and the band gap was obtained following the methodology described elsewhere [31]. In the case of P25, which has in its constitution both anatase and rutile [32], two inflection points were obtained and then two band gap values were computed – Table 3. These results are consistent with band gap values described in literature for anatase and rutile [33].

**Table 3**  
Band gap energy of photocatalysts P25 and PC500.

Samples	Band gap energy (eV)
P25	3.16/3.03
PC500	3.21

### 3.3. SEM and XRD analyses

The SEM micrographs of powder catalysts (P25 and PC500) are in agreement with manufacturer's information (Supplementary information Figs. S4 and S5), showing the primary particles of P25 with 20–30 nm particle-size and the presence of large agglomerates in the case of PC500. The commercial paint was also analyzed Fig. 8(a) – and smooth round hollow spheres were found, corresponding to a polymer extender used in this paint. Fig. 8(b) and (c) shows the morphology of photocatalytic paints #1 and #3. Photocatalyst and paint components are easily distinguished and it is visible that the photocatalyst is dispersed in the paint matrix. The photocatalytic paint with P25 seems to exhibit a better dispersion than paint with PC500 photocatalyst. However, the paint photocatalytic activity seems to be favored by a worse dispersion since more photocatalyst particles are uncoated with the polymer binder and then

“free” to react with pollutants. Deeper deagglomerated P25 photocatalyst particles (higher dispersion) make the photocatalyst to contact more extensively with the paint binder and then to competitive degradation of the paint binder and the pollutants. Indeed, UVCON tests of paints with deeper deagglomerated P25 originate more intense chalking [28]. The SEM micrographs of photocatalytic paints with calcium carbonate extender substituting pigmentary TiO<sub>2</sub> are presented in Supplementary information Figs. S6–S8.

The X-ray diffraction (XRD) patterns of titanium dioxide powders (Fig. 9) show that P25 is composed of both rutile and anatase phases, whereas PC500 is only composed by anatase phase as indicated by manufactures. P25 presents crystallites-sizes of 19 nm (anatase) and 26 nm (rutile). In the case of PC500, crystallites of 12-nm size (anatase) are found. Several authors studied the influence of crystallite size on photocatalytic performance of titanium dioxide for different photocatalytic reactions, claiming that ideal crystalline size is between 7 and 15 nm [34–36]. Smaller size crystallites lead to larger surface areas, improving pollutants adsorption and thus allowing better photocatalytic performance [37,38]. Since PC500 photocatalyst particles are smaller, a higher photocatalytic activity of this photocatalyst was expected, which is actually in agreement with the experimental results.

XRD patterns of photocatalytic paints under study are also presented in Fig. 10. Paints #1 and #3, containing 9 wt.% of pigmentary

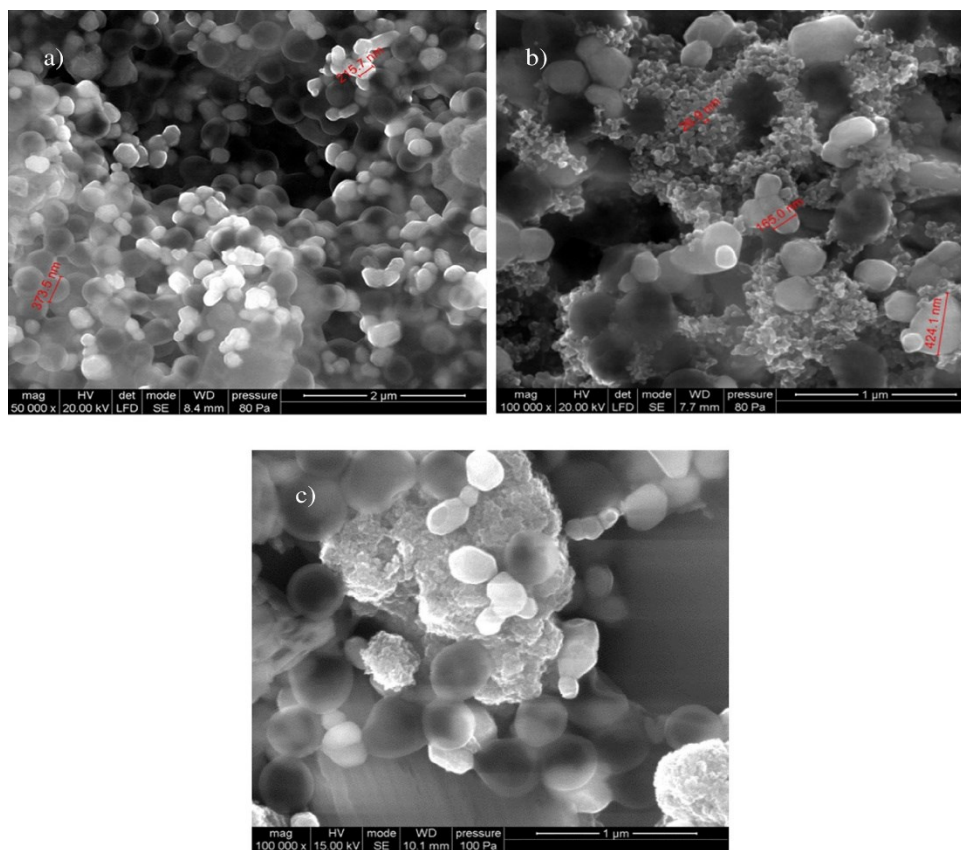


**Fig. 8.** SEM micrographs of: (a) commercial paint; (b) Paint #1; and (c) Paint #3.

TiO<sub>2</sub> and 9 wt.% of photocatalytic TiO<sub>2</sub>, were compared with a reference paint formulated with 18 wt.% of pigmentary TiO<sub>2</sub> (RP1); paints #2 and #4, which include calcium carbonate extender for substituting the pigmentary TiO<sub>2</sub>, were compared with a reference paint formulated with 18 wt.% of CaCO<sub>3</sub> (RP2). As expected, peaks corresponding to the calcium carbonate response are

observed in all spectra, being more intense for paints #2 and #4 since all the pigmentary  $\text{TiO}_2$  was replaced by  $\text{CaCO}_3$  extender. In case of paints #1 and #3, the main peak corresponding to  $\text{TiO}_2$  rutile phase ( $27.5^\circ$  and (1 1 0) facet) is higher due to the presence of pigmentary titanium dioxide (mainly rutile form).

Comparing the XRD patterns of the formulated paints with the reference paints without photocatalyst, it can be concluded that the addition of photocatalysts (P25 and PC500) does not lead to the crystalline properties change of these materials. Modifications in the crystal lattice are only observed when photocatalysts are added to the paints and the presence of the new peaks corresponding to titanium dioxide anatase for PC500 photocatalyst and anatase and rutile for P25 photocatalyst are distinguished.

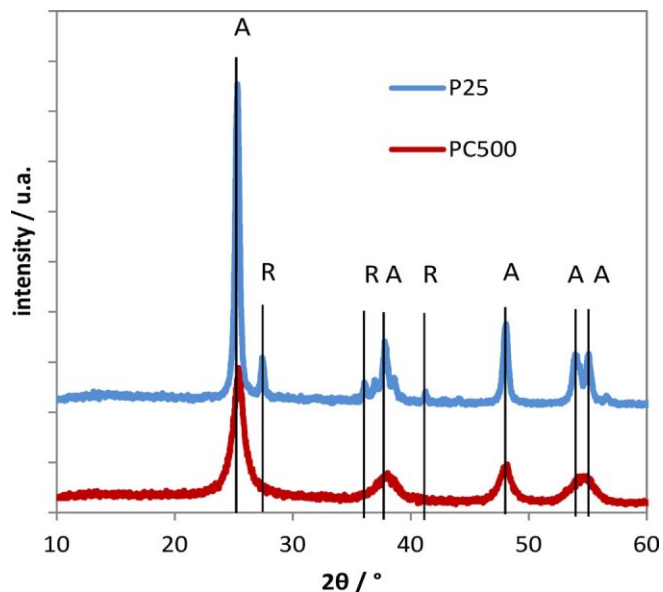


**Fig. 9.** XRD patterns for commercial titanium dioxide, P25 and PC500. The peaks corresponding to anatase and rutile phases are labeled by A and R, respectively.

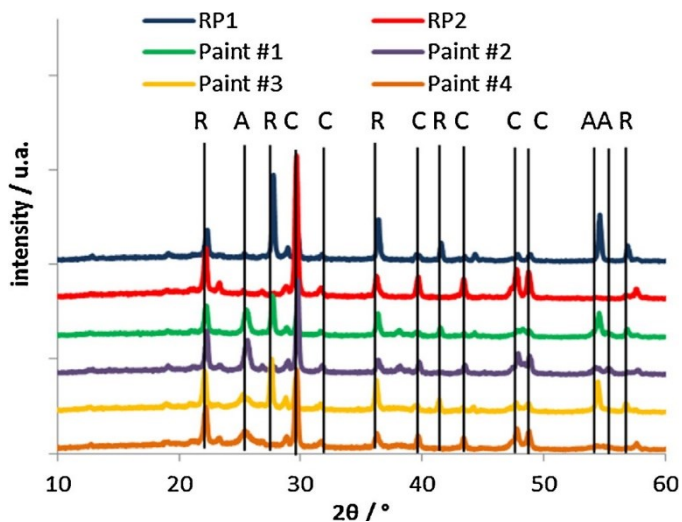


**Fig. 10.** XRD patterns for paints #1–4 and respectively reference paints (RP1 and RP2). The peaks corresponding to anatase and rutile phases are labeled by A and R, respectively. The peaks of calcium carbonate are labeled by C.

### 3.4. UVCON tests

According to QUV-A results, paints #3 and #4 presented the highest resistance to degradation. The values (scale of 0–5, being 0 a surface without chalk) of the chalking test of paints #1–4 are given in Table 4. A commercial exterior water-based paint (vinyl paint) was also analyzed for comparison purposes. Chalking is the formation of fine chalky powder on the surface of the paint, which usually indicates binder degradation. Two other parameters can be obtained from the UVCON test: cracking and color changes; the prepared paints did not exhibit crack formation nor color change.

The results obtained indicate that the best performing photo-catalytic paints (paints #3 and #4) still show some chalking effect. Besides presenting very good photocatalytic activity these paints still have to be improved concerning chalking. This can be done by changing the binder for a more resistant one towards photocatalytic oxidation.

**Table 4**

Chalking values of UVCON test.

Paint	Test duration					
	170 h	362 h	532 h	702 h	848 h	1060 h
Reference paint (without photocatalyst)	0	0	0	0	0	0
Paint #1	4	4/5	4/5	4/5	4/5	5
Paint #2	4	5	5	5	5	5
Paint #3	1	3	3	3	3	3
Paint #4	2	4	4	4	4	4

## 4. Conclusions

In the present study a commercial water-based paint was reformulated to host a photocatalyst; P25 from Evonik and PC500 from Cristal were chosen. Half of the pigmentary TiO<sub>2</sub> of the original paint was replaced by a photocatalytic TiO<sub>2</sub> and the remained pigmentary TiO<sub>2</sub> was either kept or replaced by calcium carbonate extender. Photocatalytic activity of these four paints was assessed according to the standard ISO 22197-1:2007. Comparing the best performing paints (paints #2 and #4), it can be concluded that both do not incorporate pigmentary TiO<sub>2</sub>; indeed this component blocks the light harvesting, decreasing the photocatalytic activity. Moreover, PC500-based paint (Paint #4) originates better NO conversions than P25-based paint (Paint #2), 70% and 50%, respectively, as well as it also originates better selectivities, 45% and 35%, respectively. This behavior was further studied based on SEM and XRD analyses. PC500 exhibits smaller TiO<sub>2</sub> particles compared with P25, which in principle favors the photoactivity of PC500. Moreover, the addition of photocatalysts to a paint does not introduce any changes in the original crystal lattice. Under outdoor tests, all paints showed a NO conversion higher than 80%. The best performing paint was again Paint #4 (with PC500 and calcium carbonate), presenting a NO conversion of about 95%. This validates the result obtained under lab-scale characterization.

Despite displaying some chalking, the exceptional high photo-catalytic activity of Paint #4 is ascribed to several factors: paint PVC/CPVC ratio higher than one; high paint film thickness; complete removal of the pigmentary TiO<sub>2</sub> and use of a very active photocatalyst, PC500. Paint coatings are one of the best approaches to immobilize photo-TiO<sub>2</sub> since they create a 3D layer where TiO<sub>2</sub> nanoparticles are available for photocatalysis up to the optic thickness, which is around 100 µm. Actually, the prepared paints are an example of this.

## Acknowledgements

This work is co-funded by FEDER (Fundo Europeu de Desenvolvimento Regional)/QREN (NOxOut project with reference FCOMP 01-0102-FEDER 005365) under the framework of “Programa Operacional Factor de Competitividade”. The authors also acknowledge financing from

FCT through the project PTDC/EQU- EQU/115614/2009. Joana Ângelo is grateful to the Portuguese Foundation for Science and Technology (FCT) for her PhD Grant (Reference: SFRH/BD/79974/2011). Luísa Andrade acknowledges European Research Council for funding within project BI-DSC – Building Integrated Dye sensitized Solar Cells (Contract Number: 321315) and FCT-CAPES cooperation 2013–2014. The authors would like to acknowledge Dr. Cecilia Mateos Pedrero for the fruitful discussions about XRD analyzes.

## Appendix A. Supplementary data

Supplementary material related to this article can be found, in the online version, at <http://dx.doi.org/10.1016/j.apcata.2014.07.005>.

## References

- [1] EPA, <http://www.epa.gov/> (accessed December 2013).
- [2] EEA, <http://www.eea.europa.eu/> (accessed December 2013).
- [3] K. Skalska, J.S. Miller, S. Ledakowicz, *Sci. Total Environ.* 408 (2010) 3976–3989.
- [4] M.A. Gómez-García, V. Pitchon, A. Kiennemann, *Environ. Int.* 31 (2005) 5–467.
- [5] A. Fujishima, T.N. Rao, D.A. Tryk, *J. Photochem. Photobiol. C* 1 (2000) 1–21.
- [6] S. Devahasdin, C. Fan Jr., K. Li, D.H. Chen, *J. Photochem. Photobiol. A* 156 (2003) 161–170.
- [7] Y. Paz, *Appl. Catal. B* 99 (2010) 448–460.
- [8] J.M. Herrmann, *Appl. Catal., B* 99 (2010) 461–468.
- [9] J.M. Herrmann, *Top. Catal.* 34 (2005) 49–65.
- [10] A. Masakazu, *Pure Appl. Chem.* 72 (2000) 1265–1270.
- [11] J. Chen, C.S. Poon, *Build. Environ.* 44 (2009) 1899–1906.
- [12] J. Chen, S.C. Kou, C.S. Poon, *Build. Environ.* 46 (2011) 1827–1833.
- [13] A. Folli, C. Pade, T.B. Hansen, T. De Marco, D.E. Macphee, *Cem. Concr. Res.* 42 (2012) 539–548.
- [14] L. Osburn, 5th Post Graduate Conference on Construction Industry Development, Bloemfontein, South Africa, 16–18 March 2008, 2008, p. 11.
- [15] B.Y. Lee, A.R. Jayapalan, M.H. Bergin, K.E. Kurtis, *Cem. Concr. Res.* 60 (2014) 30–36.
- [16] B. Tryba, P. Homa, R.J. Wróbel, A.W. Morawski, *J. Photochem. Photobiol. A* 286 (2014) 10–15.
- [17] T.X. Italcementi, Active the photocatalytic active principle, Technical Report, Bergamo, Italy, 2009.
- [18] A. Beeldens, Symposium on Photocatalysis, Environment and Construction Materials, RILEM Publications SARL, Florence, Italy, 2007, pp. 187–194.
- [19] T. Maggos, A. Plassais, J.G. Bartzis, C. Vasilakos, N. Moussiopoulos, L. Bonafous, *Environ. Monit. Assess.* 136 (2008) 35–44.
- [20] G.L. Guerrini, *Constr Build Mater* 27 (2012) 165–175.
- [21] EDSA, B.P., <http://boysenknoxoutproject.com/> (accessed December 2013)

- [22] T. Maggos, J.G. Bartzis, M. Liakou, C. Gobin, *J. Hazard. Mater.* 146 (2007) 668–673.
- [23] N.S. Allen, M. Edge, J. Verran, J. Stratton, J. Maltby, C. Bygott, *Polym. Degrad. Stab.* 93 (2008) 1632–1646.
- [24] E. Claire, Bygott, E. Julie, Maltby, L. John, R. Stratton, McIntyre, *Symposium on Photocatalysis, Environment and Construction Materials*, RILEM Publications SARL, Florence, Italy, 2007, pp. 251–258.
- [25] Boysen, <http://www.knoxoutpaints.com/> (accessed December 2013).
- [26] Light2Cat, <http://www.light2cat.eu/> (accessed May 2014).
- [27] S. Suárez, R. Portela, M.D. Hernández-Alonso, B. Sánchez, *Environ. Sci. Pollut. Res. Int.* (2014), <http://dx.doi.org/10.1007/s11356-014-2725-y>.
- [28] C. Águia, J. Ângelo, L.M. Madeira, A. Mendes, *J. Environ. Manage.* 92 (2011) 1724–1732.
- [29] C. Águia, J. Ângelo, L.M. Madeira, A. Mendes, *Catal. Today* 151 (2010) 77–83.
- [30] S.I. Boldish, W.B. White, *Am. Mineral.* 83 (1998) 865–871.
- [31] A.B. Murphy, *Sol. Energy Mater. Sol. Cells* 91 (2007) 1326–1337.
- [32] B. Ohtani, O.O. Prieto-Mahaney, D. Li, R. Abe, *J. Photochem. Photobiol. A* 216 (2010) 179–182.
- [33] Y.V. Pleskov, *Russ. J. Electrochem.* 39 (2003) 328–330.
- [34] S. Liu, N. Jaffrezic, C. Guillard, *Appl. Surf. Sci.* 255 (2008) 2704–2709.
- [35] Q. Zhang, L. Gao, J. Guo, *Appl. Catal. B* 26 (2000) 207–215.
- [36] A.J. Maira, K.L. Yeung, C.Y. Lee, P.L. Yue, C.K. Chan, *J. Catal.* 192 (2000) 185–196.
- [37] M. Xie, L. Jing, J. Zhou, J. Lin, H. Fu, *J. Hazard. Mater.* 176 (2010) 139–145.
- [38] J. Jiu, F. Wang, M. Adachi, *Mater. Lett.* 58 (2004) 3915–3919.